11th Europhysical Conference on Defects in Insulating Materials (EURODIM 2010) IOP Publishing
IOP Conf. Series: Materials Science and Engineering **15** (2010) 012013 doi:10.1088/1757-899X/15/1/012013

Paramagnetic signature of microcrystalline silicon carbide

A. Konopka[1], B. Aşik[2], U. Gerstmann[1], E. Rauls[1], N.J. Vollmers[1], M. Rohrmüller[1], W.G. Schmidt[1], B. Friedel[3], and S. Greulich-Weber[1]

[1]University of Paderborn, Department of Physics, Paderborn, Germany
[2]Physics Department, Çankırı Karatekin University , Çankırı, Turkey
[3]Cavendish Laboratory, Dep. of Physics, University of Cambridge, Cambridge CB3 0HE, UK

E-mail: greulich-weber@physik.upb.de

Abstract. The most important challenge on the way to optimized solar cells is to make the thickness of the individual layers smaller than the diffusion length of the charge carriers, in order to keep the collection efficiency close to unity. Here, we propose *ß*-SiC microcrystals grown by a sol-gel based process as a promising acceptor material. The samples are characterized by optical spectroscopy and electron paramagnetic resonance (EPR). With the help of band structures for selected surface states calculated in the framework of density functional theory (DFT) a possible scenario for the observed acceptor process is discussed.

1. Introduction

Hydrogenated nano- and micro-crystalline silicon carbide (*nc*-SiC:H and *μc*-SiC:H) have become an attractive new class of advanced microstructured materials for heterojunction photovoltaic devices and light emitting diodes. This interest is due to their wide band gap and lower absorption in the visible region while retaining their higher conductivity. The high optical band gap of SiC makes this material also suitable as window layers in solar cells or even allows the replacement of TCO (transparent conducting oxides) materials. One can then further proceed to a successive deposition of hydrogenated nano-crystalline layers of silicon and of silicon carbide, aiming at the fabrication of *nc*-SiC:H/*nc*-Si:H hetero-structures [1, 2], thus, covering a broader excitation spectrum than conventional silicon cells. The result is a considerably increased efficiency of the aimed solar cell. The diffusion lengths of electrons and holes in *μc*-Si:H are around 1 μm and are, thus, insufficient to ensure satisfactory charge collection in devices which are a few μm thick. As a result, drift-assisted collection of the photo-generated carriers is needed. Here one possibility is the use of nominally undoped material as a photovoltaically active layer in analogy to amorphous silicon cells. This configuration is called a *p-i-n* structure [1, 2], where an intrinsic (*i*) photoactive semiconducting layer is surrounded by two semiconductor layers, (*p*) and (*n*), respectively, having larger bandgaps than the intrinsic layer.

Moreover, wide-bandgap microcrystals are also of interest as effective charge carrier collectors in organic solar cells. The charge separation mechanism in organic solar cells is different from that in inorganic semiconductor devices. Organic materials are covalent solids without electron overlap, and there are no electron and hole carriers in the traditional sense. In the absence of light there are no charge carriers if two organic semiconductors are brought into contact. When a photon is absorbed by an organic photoactive material, an exciton, i.e., a bound state of an electron and a hole, is created. This neutral quasi-particle has a – compared to inorganic semiconductors – notably short life time of

several tens' of nanoseconds. The most important design criterion in this kind of solar cell is to make the thickness of the individual layers smaller than the diffusion length of the exciton, in order to keep the collection efficiency close to unity. To generate electricity, the exciton has to dissociate into an electron and a hole. Overcoming Coulomb attraction of photo-generated species becomes possible at heterojunction of two organic materials: donor and acceptor. One approach to achieve an efficient charge carrier generation in polymer-based light absorbers is to blend them with suited acceptors. Upon photoexcitation an ultrafast electron transfer between a donor and a proximate acceptor takes place. This ensures an efficient charge generation with quantum efficiency close to unity [3, 4]. One of the most extensively studied device concepts, so far, is based on the bulk heterojunction approach [5]. Here, the fullerene molecules (PCBM in Figure 1) are dispersed in a polymer matrix (P3HT in Figure 1). The thin photoactive film is then sandwiched between two electrodes with asymmetric work functions forming ohmic contacts to the respective *p*- and *n*-type semiconductors (PEDOT respectively ITO and Al in Figure 1). Amongst others one approach to increase the efficiency of this kind of solar cells is to use alternative acceptor materials with a suitable position of the LUMO (lowest unoccupied molecular orbital) level. By adjustment of the latter the open circuit voltage of the solar cell can be increased at the expense of the energy lost by the electrons connected with charge transfer from donor to acceptor material. Instead of using rather expensive fullerenes, currently wide bandgap micro and nano-crystals as acceptor materials are under discussion, such as TiO_2 [6], ZnO [7], and SiC [8] (see Figure 1 for 3C-SiC). In order to optimize the function of the solar cell, individually control on doping of wide bandgap microcrystals is necessary. Usually the mentioned materials provide unavoidable technical difficulties, such as omnipresent *n*-doping, intrinsic defects or the lack of suitable *p*-doping. Thus, essential conditions concerning the acceptor materials are well adapted doping, well understood intrinsic defects, and their control in order to fit electrical levels for optimal charge separation and function of the solar cell.

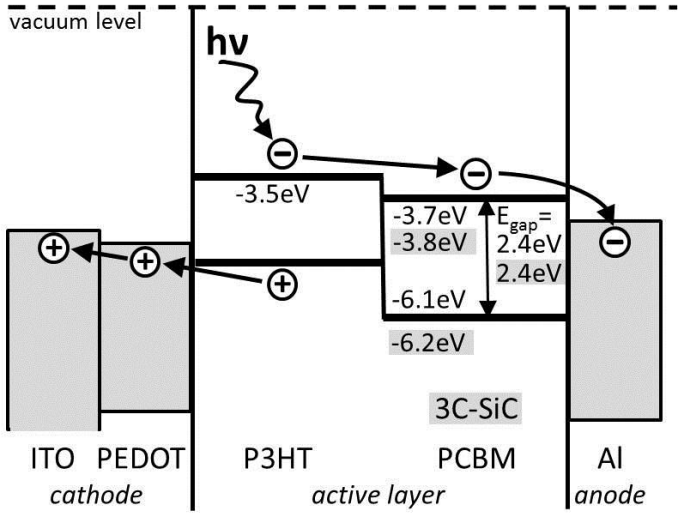

Figure 1. Schematic energy level diagram for P3HT:PCBM blend organic solar cells with ITO/PEDOT: PSS and Al as electrodes. The exciton is generated by sun light in a blend of poly(3-hexylthiophene) (P3HT) and fullerenes (PCBM), where PCBM acts as an electron acceptor and provides interface and work function energy for charge separation. As an alternative acceptor of *μc*-3C-SiC levels relative to the vacuum level are given.

In this work, we propose *ß*-SiC microcrystals grown by a sol-gel based process as a promising acceptor material instead of fullerenes (see Figure 1 for highlighted values of 3C-SiC). Our paper is organized as follows: We first present details of the sample preparation. Afterwards the samples are characterized by optical spectroscopy and electron paramagnetic resonance (EPR). With the help of band structures for selected surface states calculated in the framework of density functional theory (DFT) a possible scenario for the observed acceptor process is discussed. Finally, *ab initio* calculated EPR parameters, hyperfine splittings as well as the electronic *g*-tensors are shown to be sensitive quantities: e.g. the resolved hyperfine splittings around 30 MHz indicate that at least one of the corresponding EPR signals originates from a dangling-bond like state at a carbon- terminated surface.

2. Sample preparation

Several reports have been published [9, 10] on the preparation of *μc*-SiC:H, e.g. by electron cyclotron resonance, plasma enhanced chemical vapor deposition, and hot wire chemical vapor deposition below 300°C. All these techniques, however, are associated with a number of problems concerning homogeneity, unavoidable intrinsic and extrinsic defects, and especially arbitrary doping. Thus, as an alternative, we propose a sol-gel process for growing high purity microcrystalline 3C-SiC and 3C-SiC films allowing arbitrary doping with donors and acceptors [11]. Details of the sol-gel SiC process are given elsewhere [11]. Unlike customary SiC, sol-gel based SiC does not contain any unwanted contamination such as the omnipresent nitrogen donor in customary SiC. Thus, sol-gel SiC is semi-insulating and needs further doping if necessary for electronic or optical applications. As probing dopants, we have used phosphorous, nitrogen, boron, and aluminium, which are the technologically most requested ones concerning 'conventional' semiconductor SiC and are well known from different characterization methods. In contrast to commercially available SiC, with our method *p*-type doping and semi-insulating properties are possible without nitrogen donor compensation or activation of intrinsic defects, respectively. In all above mentioned procedures foreign ions can be introduced in two different ways. The dopant can be added during SiC precursor preparation, by adding either itself or a soluble compound to the initial solution. Suitable candidates are nitrates (N doping), borates (B), phosphates (P) or chlorides (e.g. for Al). During degradation of the precursor and during annealing at 1800°C, the foreign ions are automatically built-in into the growing SiC crystal structure. The other more difficult way is providing the dopant via gas phase during the high temperature annealing process (e.g. nitrogen). Although this method is only suitable for selected elements, also other doping elements are possible, but not yet tested.

In the present study we used samples with 1μm diameter, controlled by electron microscopy. The obtained microcrystalline samples are intended to be hydrogen-free in this study. In order to proof successful incorporation of dopants we used electron paramagnetic resonance (EPR) and optical spectroscopy.

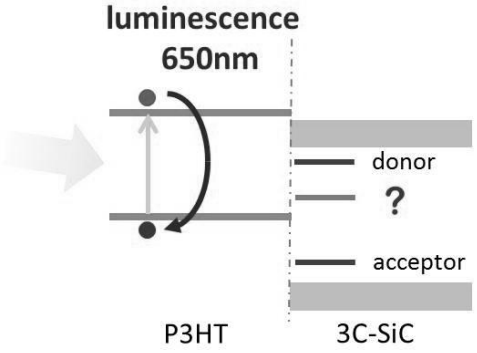

Figure 2. Part of the diagram of figure 1 with *μc*-3C-SiC acting as acceptor in the polymer taking into account different Fermi levels if the material is doped by either N donors or Al acceptors and intrinsic defects. The fast recombination of the exciton yields a luminescence centred at 650 nm which is at least partly suppressed by the dissociation of the exciton at *μc*-3C-SiC.

In the following we restrict the results of our study to shallow acceptor doping of 3C-SiC with aluminium, since we observed the strongest increase of photovoltage by using blends of the photoactive polymer and Al-doped μc-3C-SiC. If an exciton is created in the polymer, a fast recombination luminescence is observed at around 650 nm (see Figure 2 and 3). In a blend of polymer and 3C-SiC microcrystals this recombination is suppressed if the work function of the microcrystal is larger than the binding energy of the exciton. Thus, if the Fermi level of the microcrystal determines the work function, appropriate SiC doping might optimize the charge separation for the photovoltaic process. The suppression of the recombination luminescence upon increasing Al acceptor concentration is shown in Figure 3. The maximum luminescence quenching was achieved at 1·1019cm-3 Al doping. Higher doping levels did not increase the quenching, whereby surprisingly nominally undoped microcrystalline sol-gel 3C-SiC shows already the same luminescence quenching. However, no change in lumines-

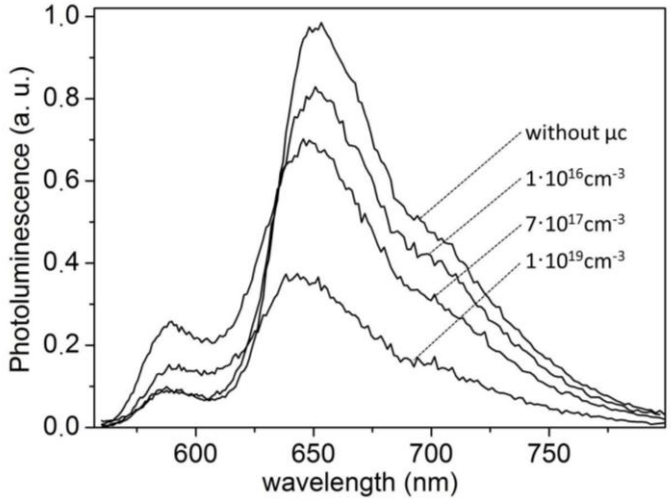

Figure 3. Suppression of the recombination luminescence in a P3HT:μc-3C-SiC blend upon Al acceptor doping of μc-3C-SiC. The luminescence was normalized to the polymer that contains no microcrystals.

cence intensity was observed upon N donor doping. In conclusion, the expected 100% luminescence quenching was not achieved with the present 1µm 3C-SiC crystals. Thus, the open questions are, whether unknown defects determine the Fermi level and if surface or interface defects are important, and whether luminescence quenching can be optimized by size control.

3. Experimental characterization.

As an analytic tool for the investigation of defects and dopants in microcrystalline 3C-SiC we used electron paramagnetic resonance (EPR). As a representative example figure 4 shows the EPR spectrum of Al-doped 1µm-sized 3C-SiC prepared by the sol-gel method. In Figure 4, also EPR 'stick' spectra of known defects and dopants in μc-SiC (bulk material) are plotted. However, none of the known spectra explains the observed EPR. Unambiguously, these nano-crystals do not contain nitrogen (labelled N in Figure 4) as was already expected from crystal growth. Further defects, like vacancies [12] (V_{Si}^- in Figure 4) or the series of interface-related defects ($D_{I\text{-}IV}$ in Figure 4) observed in [13] are not present. Unfortunately, the EPR of the Al acceptor in 3C-SiC is not known. However, in 4H-SiC and 6H-SiC always relatively broad lines and large g-factors (4H: $g_{\|}$ =2.35 and 6H: $g_{\|}$=2.4178, 2.4043, 2.3357 for 3 inequivalent sites [14]) were observed for $B||c$ while for $B\perp c$ the signal vanished (see e. g. [14]). Therefore, the broad line labelled 'C' in Figure 4 could be a candidate for Al in 3C-SiC, at least for an Al-related center. Two further spectra labelled 'A' and 'B' were observed and analysed using the usual Spin-Hamiltonian (for the resulting parameters, see Table 1). They are completely unknown from bulk material and, thus, most probably surface related. To unravel their microscopic origin we need comparative theoretical data.

4. Theoretical modelling and discussion

In order to elucidate the microscopic origin of the observed EPR signals, we perform first principles calculations of the EPR parameters. The calculations are based on density functional theory (DFT) using the gradient-corrected PBE functional in its spin-polarized form. For a modelling of the surfaces we use supercells and periodic boundary conditions. To calculate the electronic g-tensor we use linear magnetic response theory. Hence, an explicit treatment of the external magnetic field is necessary, and in order to retain the translation invariance of the wave functions, this has to be done in a gauge-invariant way. The gauge-including projector augmented plane wave (GI-PAW) approach satisfies this requirement using an efficient pseudopotential approach [16, 17]. The hyperfine splittings are calculated taking into account relativistic effects in scalar-relativistic approximation. Recently, the GI-PAW approach has been implemented in the pwscf-code (QUANTUM-ESPRESSO package) [18] and has been already applied successfully to investigate paramagnetic structures in bulk material and partially

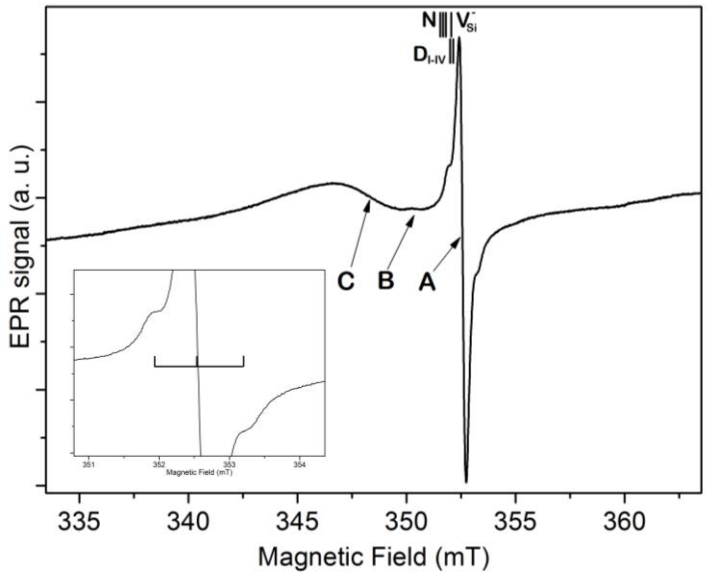

Figure 4. X-band EPR measurement performed at 8 K on Al-doped μc-3C-SiC prepared by a sol-gel method. The magnetic field positions labelled A, B, and C determine the centres of gravity of the resonances (g-factors). Their values are summarized in table 1. The inset shows the central resonance A with hf splitting as given in table 1 marked with bars. The figure also shows the line positions of known defects such as the N donor [12], the silicon vacancy [12] and further intrinsic defects labelled D [13].

hydrogenated surfaces of silicon [19]. To model the surfaces of the SiC microcrystals, we use similar settings as for silicon in Ref. 19. Seven atomic layers (four Si and four C, each) are treated in a supercell with up to 145 atoms, whereby the lowest layer was saturated with H atoms (see also Figure 5a and 5b). To ensure a well-defined transition to bulk material, the atoms in the lowest three layers (one Si-C double layer and the H saturation layer) were kept on their ideal bulk positions. All other atoms were allowed to relax freely. To minimize the interaction of the periodic images of the surface, 10 Å vacuum is inserted. We use norm-conserving pseudopotentials with a plane wave energy cutoff of 50 Ry. Whereas for the geometry optimisation a 2x2x1 Monkhorst-Pack (MP) *k*-point set comes out to be sufficient, to obtain reasonably converged estimates for the *g*-tensor, at least 4x4x1 samplings are unavoidable (see Ref. 19).

As first reference systems we briefly discuss the (001) surfaces of 3C-SiC and related materials: in silicon, the most stable reconstruction of the clean surface is characterized by rows of buckled dimers, which are still surviving if the surface is partially hydrogenated. Only, if nearly all silicon atoms are mono-hydrogenated, the dimers at the reconstructed surface lose their buckling. In 3C-SiC, the silicon-terminated (001) Si-surface looks very similar at first view. However, it is well known that due to the smaller bond length in SiC the buckling becomes less efficient: According to our total energy calculation the adsorption of a single H-atom is sufficient to destroy the buckling, resulting in metallic and diamagnetic properties of the reconstructed surface. Hence, this configuration cannot be responsible for the observed paramagnetic structures. Besides this 2x1 dimer reconstruction there are a lot of other more complicated reconstructions [20], that are, however, not well suited as first reference systems.

Table 1. Spin-Hamiltonian parameters (effective *g*-tensors, line widths, and in case of spectrum 'C' also a resolved hf splitting due to 4-5 more or less equivalent Si nuclei) extracted from the spectra shown in Figure 4. Experimental errors are *g*: 0.00005, line width: 0.02 mT, and *A*: 0.02 MHz for spectra A and B. The experimental errors for spectrum C are: g: 0.0005, line width: 0.05.

spectrum	*g*	line width [mT]	hf splitting *A* [MHz]
A	2.0001	-	26.40
B	2.0095	0.94	-
C	2.0256	4.72	-

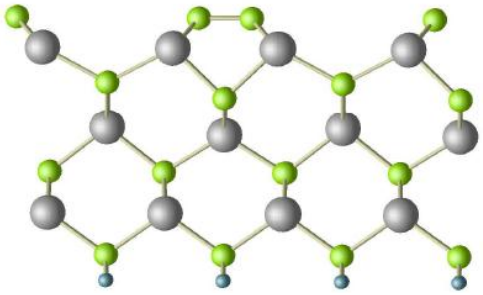

Figure 5a. "clean" SiC (001) surface with dimer reconstruction. Silicon big balls and carbon medium balls.

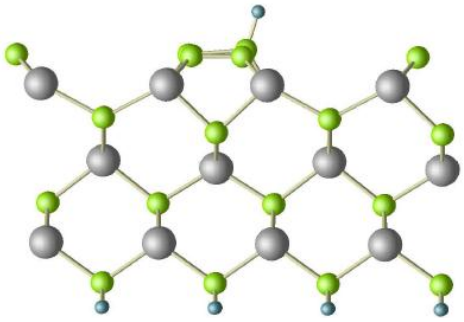

Figure 5b. SiC (001) surface with one hydrogen atom in Si reconstruction. Silicon big balls, carbon medium balls and hydrogen small balls.

They are, thus, beyond the scope of this work. Instead we focus onto the carbon-terminated c-surface, where the situation is by far more straightforward. Here, similar to the case of diamond, already the clean surface provides a 2x1 dimer reconstruction *without* buckling (see also Figure 5a).

Figure 6 (*center*) shows the resulting band structure: in comparison with SiC-bulk material (*left part*) additional broad bands appear in the gap. Those in the lower part are occupied covering a 1.2 eV broad region. The unoccupied bands overlap with the conduction bands of the bulk material. Altogether, the fundamental gap is considerably reduced to 0.2 eV. The result is an auto-doping of the 3C-SiC microcrystals. If a single H-atom is adsorbed at the formerly clean SiC (001) c-surface (see also Figure 5b), the double bond of the adsorbing dimer is broken. That C-atom to which the H-atom bounds, is lifted a little bit. The second C-dimer atom remains more or less on its former position, but contains an

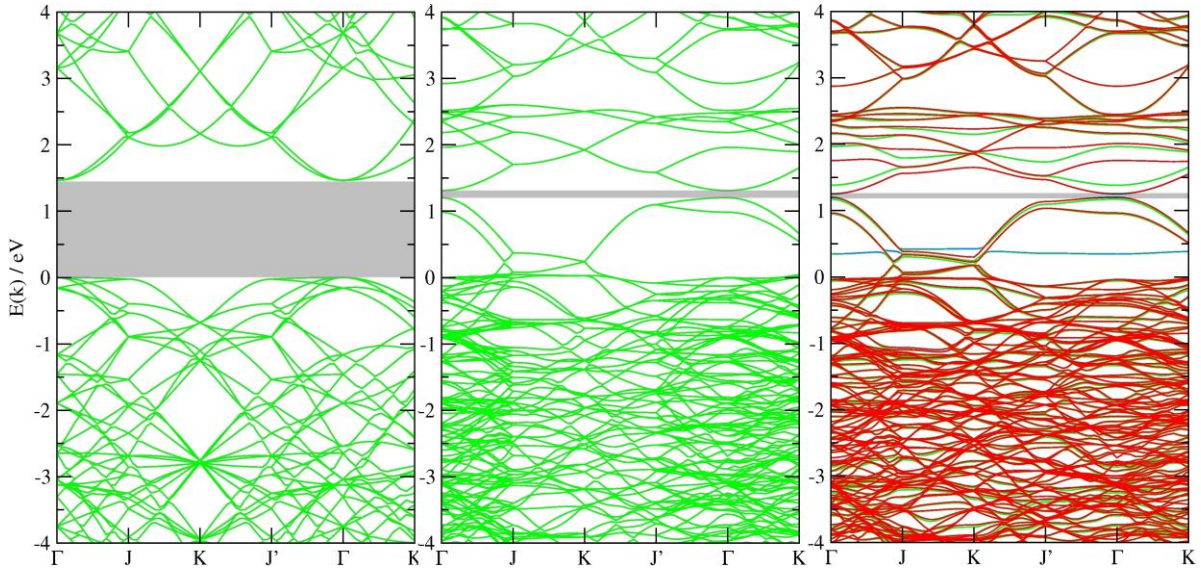

Figure 6. Calculated band structure of 3C-SiC bulk (*left*) and for a 2x1 dimer-reconstructed SiC (001) c-surface (*central*). The band structure for the same surface, but with an H-atom adsorbed as shown in Figure 5b) is also given (*right*, spin-up and spin-down electrons in green and red, respectively). The reduction of the fundamental gap (*shaded grey*) by the surface leads to an efficient auto-doping.

unpaired electron in a dangling bond (db)-like orbital. This unpaired electron dominates the electronic structure that becomes, thus, paramagnetic. Therefore, the corresponding band structure is spin-polarized (see Figure 6, *right*), but contains otherwise all features of the band structure of the clean surface. Moreover, an additional occupied band 0.4 eV above the bulk-like valence bands is induced by this paramagnetic defect. It shows only minor dispersion, indicating the localized, db-like character of this defect level. In both cases the gap is significantly reduced, and the existence of the surface leads to an efficient auto-doping. In other words, already the nominally undoped microcrystalline sol-gel 3C-SiC behaves as an efficient acceptor for the charge carriers collection.

The band structure of the surfaces explains also the behavior of photovoltage with respect to additional, intentional doping: doping with Al acceptors may shift the Fermi level slightly towards the valence bands, however, does not change considerably the situation in comparison to undoped μc-SiC. Doping with donors (e.g. nitrogen), on the other hand, is even counteracting, since the Fermi level lies at least between those surface induced states and the shallow donor level. Thus, the surface-induced states are filled by shallow donor electrons. The consequence is a less attractive 'acceptor' for charge separation (dissociation of the exciton), since most surface states are already occupied.

According to our DFT linear magnetic response calculations, the paramagnetic dangling-bond-like defect SiC(001)+H explains not only the observed high collection efficiency. This defect structure also fits the hf structure of spectrum A, experimentally observed in Al-doped μc-3C-SiC prepared by our sol-gel method. Most of the magnetization density is localized at the db-like C-Atom at the surface, giving (see Figure 5b) rise to a large hf splitting of about 360 MHz (parallel to the surface normal, see Table 2). However, due to its very small natural abundance of about 1%, there is no chance to resolve the corresponding or any other C-related hf satellite lines. The only hf lines that can be resolved are Si-related. According our calculations, the largest splittings originate from the first Si-layer below the C-terminated surface: With a value of 29.4 MHz (Si_{db}) and -32.8 MHz (Si_H) the four Si-atoms below the db-C-C-H dimer provide hf splittings in nice agreement with the experimentally observed values due to 4 - 5 more or less equivalent Si nuclei. Note that the EPR experiment cannot distinguish between the different signs.

The calculated *g*-tensor, however, does by no means agree with the experimental value for EPR signal A, measured in Al-doped μc-3C-SiC. From the calculated main values (g_1=2.0034, g_2=2.0027, g_3= 2.0029) we obtain an angular average of about 2.0030, far away from 2.0001 measured for signal A (see also Table 1).

5. Summary and outlook

Our study shows that sol-gel grown micro- and nano-crystalline 3C-SiC can serve as an excellent acceptor material for an effective charge separation in organic solar cells. As an unavoidable add-on in polymer blends it fits excellently into the energy level scheme of these kind of solar cell and has the potential to replace the usually used rather expensive fullerenes. It turned out, that undoped μc-3C-SiC

Table 2. Hyperfine splittings calculated from first principles for the paramagnetic surface state originating from a single H-atom adsorbed at 2x1 dimer-reconstructed SiC(001) c-surface. θ denotes the angle between the main axis of a given hf tensor and the surface normal (001).

nuclei	A_1 [MHz]	A_2 [MHz]	A_3 [MHz]	$A_{\parallel}$(001)	θ
H	51.4	52.1	64.6	55.2	60.5°
C	- 1.9	-3.0	-5.3	-4.8	17.1°
C(db)	176.1	178.1	377.6	359.2	16.3°
2xSi_{db}	29.8	26.5	23.2	29.4	80.4°
2xSi_H	- 29.6	-30.3	-35.8	-32.8	31.1°

acts as a particular suitable acceptor due to its auto-doping mechanism by a surface-induced band structure. This behaviour could not be observed in any other micro- or nano-crystalline SiC known so far, since they all contain the omnipresent and unavoidable shallow nitrogen donor. Only the developed sol-gel SiC growth allows the preparation of nitrogen-free SiC. In order to discover in detail the microscopic origin of the outstanding collection efficiency, comparative theoretical *ab initio* data seems to be unavoidable. First reference calculations of the EPR parameters indicate, that the *g*-tensor is by far more sensitive than the hf splittings. A very small *g*-value of 2.0001 far below the free-electron value of g_e=2.0023 seems to be very characteristic and indicates an exceptional acceptor-like electronic structure of the responsible microscopic structure. It appears as a very characteristic feature and should be the basic key for structure identification remaining for next future work.

Acknowledgement. Part of the work was supported by TUBITAK (The Scientific and Technological Research Council of Turkey).

References

[1] Y. Hamakawa, Y. Tawada, Int. J. Solar Energy, Vol. I, pp. 125-144 (1982).
[2] Y. Matsumoto, G. Hirata, H. Takakura, H. Okamoto, and Y. Hamakawa J. Appl. Phys. **67,** 10 (1990).
[3] N.S. Sariciftci, L. Smilowitz, A.J. Heeger, F. Wudl, Science **258**, 1474 (1992).
[4] C.J. Brabec, G. Zerza, G. Cerullo, S. De Silvestri, S. Luzatti, J.C. Hummelen, N.S. Sariciftci, Chem. Phys. Lett. **340**, 232 (2001).
[5] G. Yu, J. Gao, J.C. Hummelen, F. Wudl, A.J. Heeger, Science **270,** 1789 (1995).
[6] Q. Fan, B McQuillin, DDC Bradley, S Whitelegg, AB Seddon, Chemical Physics Letters **347**, 325–330 (2001).
[7] J. J. Cole, X. Wang, R. J. Knuesel, and H. O. Jacobs, *Nano Lett.,* **8**, 1477 – 1481, (2008).
[8] S. Ogawa, Applied Physics **46**, 518–522 (2007).
[9] A. Dasgupta, S.Ghosh, S.Ray, Journal of Materials Science Letters **14**, 1037 (1995).
[10] S. Miyajima, K. Haga, A. Yamada and M. Konagai, Japanese Journal of Applied Physics **45**, L432 (2006).
[11] B. Friedel and S. Greulich-Weber, Materials Science Forum **527-529**, 759-762 (2006)
[12] W. E. Carlos, in G. L. Harris (Ed.), *Properties of Silicon Carbide*, INSPEC, Stevenage, p. 42 (1995).
[13] A. Kassiba , M. Makowska-Janusik , J., Boucle, J.F. Bardeau, A. Bulou, N. Herlin, M. Mayne, X. Armand, Diamond and Related Materials **11** 1243–1247 (2002).
[14] S. Greulich-Weber, phys. stat. sol. (a) **Volume ??**, 162 95 (1997).
[15] H.J. von Bardeleben, J.L. Cantin, L. Ke, Y. Shishkin, R.P. Devaty and W.J. Choyke, Mat. Sci. Forum **483-485**, 273 (2005).
[16] Ch.J. Pickard and F. Mauri, Phys. Rev. B **63**, 245101 (2001).
[17] Ch.J. Pickard and F. Mauri, Phys. Rev. Lett. **88**, 086403 (2002).
[18] P. Giannozzi et al., *J. Phys.: Condens. Matter* **21,** 395502 (2009); http://www.quantum-espresso.org.
[19] U. Gerstmann, M. Rohrmüller, F. Mauri, and W.G. Schmidt, phys. stat. sol. (c) **7**, 157 (2010).
[20] V. Yu. Aristov, phys. usp. **44**, 761 (2001).